A case study on lightning protection, current injection measurements, and model

A Case Study on Lightning Protection, Current Injection Measurements, and Model

Geesje Bargboer, *Student Member, IEEE*, and Alexander P. J. van Deursen, *Senior Member, IEEE*

***Abstract*—A newly built pharmaceutical plant has been investigated by measurements. Currents of 0.3 kA were injected in the lightning protection grid on the roof. Inside the building, test cables of 100 m length followed a path typical for cables belonging to the installation. We measured induced cable currents and voltages. A reduced model of the building incorporated most of the designed current paths. Measurements and model showed that the roof steel skeleton carried about 80% of the current and the intended lightning conductors 20%. The calculated current through a cable support was larger than measured. This is explained by also considering a nearby nonintended conductor. For three types of cables, we determined the transfer impedances. The measurements and model have been combined and extrapolated to actual lightning.**

***Index Terms*—Current injection, experimental methods, lightning protection (LP), verification.**

I. Introduction

LIGHTNING protection (LP) design is often based on rules derived from practical experience and sound reasoning [1]. Periodic visual inspection of the LP system is recommended, with tests on the resistance to ground. For high-risk buildings or structures and buildings with a large economic value, it would be advisable to test the whole building with current injection, but such tests are not foreseen in [1, Part 1, Annex. D]. A well-known exception is the certification procedure for airplanes. The injection current should have a sufficient amplitude and sufficiently short rise time to resemble the real threat. These requirements are hard to meet for a large structure, such as a building. A workaround is possible when the major part of the protection relies on metallic conduction. In this case, the protection behaves linearly unless arcing-over changes current paths. The tests can be performed with a current of lesser amplitude, and lightning induced currents and voltages can be obtained by extrapolation. Small currents also avoid damage to inadequately protected equipment during tests. Nevertheless, the injected current should have a sufficiently high-frequency content to be representative of lightning. The current distribution in the building depends on the internal and external impedances of the conductors. The external impedances are inductive, and dominate the internal even taking the skin effect of steel into account (see also Section IV-A). As a result, the frequency is a common factor for all relevant impedances. The current distribution then does not strongly depend on frequency, until resonances show up. The measurement frequency of 18.4 kHz lies within this range for the building studied; the first resonance occurs at 0.9 MHz. The first quarter sinewave has a duration of 9 μs, which compares reasonably well with the rise time of the first stroke in [1, Part 1, Annex. A].

LP is usually described in terms of routing of large currents, reduction of magnetic fields, and induced voltages in large open loops [1]–[4]. A complementary approach focusses on currents and reduction of the transfer impedance Z_t. Inside the building, all cables are supported by metal ladders and trays that form a continuous conducting structure integrated with the LP. This way of interconnection has been advised before and implemented during construction. The support acts as an "earthed parallel conductor" (EPC) [5]–[8] and protects the cables and electronic equipment. Many cables have protective earth (PE) leads, shields, or armors as additional EPC. The voltages at equipment terminals are then related to the induced cable common-mode (CM) current via the Z_t. The Z_t varies largely between cables and is a function of frequency for each cable. The open-loop voltage does not appear at equipment terminals when the EPCs are connected to the local ground at both ends. But it would do so without EPC or with EPC disconnected at either end.

Whether the total industrial system is lightning safe depends also on the equipment connected to the cables. This is outside the scope of the paper. The aim is to investigate to what extent a limited model of a complex building agrees with the measurements performed, what the benefits of armored and shielded cable are, and what a tentative extrapolation to lightning gives. Numerous papers appeared on the distribution of lightning currents in buildings with steel structures, e.g., [9] and references therein. Often the structures studied are less complicated than actual industrial installations.

Some of the data in this contribution have been presented earlier in preliminary reports [10], [11]. This paper adds more elaborate modeling and a more detailed comparison with measurements.

II. Building and Measurement Setup

The four floor building of 69 m (w) $\times$ 72 m (b) $\times$ 21 m (h) is a new plant for the production of medicines. The measurements were requested after the building was constructed and most of the electrotechnical installation was completed. Fig. 1 shows

Manuscript received September 1, 2009; revised February 1, 2010 and March 15, 2010; accepted April 24, 2010; Date of publication June 14, 2010; date of current version August 18, 2010. This work was supported by the Dutch Ministry of Economic Affairs of the Innovation Oriented Research Program–Electromagnetic Power Technology under Project 2301A.

The authors are with the Department of Electrical Engineering, Eindhoven University of Technology, Eindhoven, MB 5600, The Netherlands (e-mail: g.bargboer@tue.nl; a.p.j.v.deursen@tue.nl).

Color versions of one or more of the figures in this paper are available online at http://ieeexplore.ieee.org.

Digital Object Identifier 10.1109/TEMC.2010.2050486

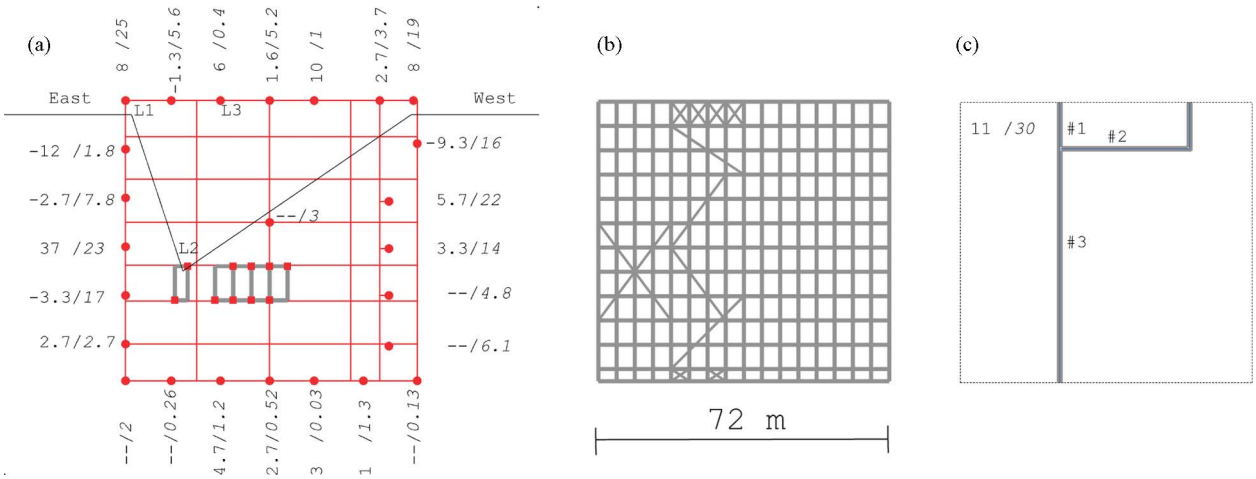

Fig. 1. Three horizontal layers. (a) Roof grid at 19 m height with source position and HV leads indicated; the dots show the connections between roof grid and steel skeleton. Currents between grid and skeleton at the building edge and middle point are indicated (measured/*calculated*). (b) Top of the steel skeleton at 18.5 m height. (c) Cable support path at 16 m height. The lightning attachment positions L1, L2, and L3 in (a) and branches #1, #2, and #3 in (c) are discussed in Sections II and V.

the layout of relevant conductors on the roof and the fourth floor with air treatment installations. To intercept the lightning current, a coarse grid of 50 mm^2 copper wire on the roof is assisted by a large number of 3 m tall rods [see Fig. 1(a)]. A steel skeleton gives the top floor its structural strength and supports the concrete roof plates [see Fig. 1(b)]. The grid is connected to the steel skeleton at many points on the edge of the roof, at a few points near the air-cooling units on the roof, and at midroof [dots and squares in Fig. 1(a)]. At the facades, the steel skeleton rests on reinforced concrete poles and is connected to downconductors leading to the foundation grounding. A buried ring around the building and rod electrodes placed at approximately 12 m spacing complete the outer LP. The total resistance to earth is smaller than 1 Ω. Inside the building, interconnected metal ladders and trays support the cables. The part on the fourth floor shown in Fig. 1(c) is typical for all other paths, only the horizontal extension is displayed. Two bundles of four 100 m long test cables have been laid for the measurements. The selection contained data and power cables, shielded, armored or unshielded, all of them samples of those used in the actual installation. One bundle ran over support branches #1 and #3, the other over #2 and #3. Near the facades, the cables followed a vertical path downward over the distance of 2, 15, and 15 m at the ends of branch #1, #2 and #3, respectively.

The current source was placed on the roof, at the frame of a spare location for an air-cooling machine. Four short steel pillars carried the frame and connected it to the skeleton. At opposite edges, the frame was connected to the roof grid (see Fig. 2). A 0.5 μF, 40 kV capacitor was the current source; a spark gap acted as switch. The "cold side" of the source was connected to the frame. From the "hot side" long Filotex high-voltage (HV) leads ran at 2.5 m above the roof toward two grounding electrodes at 50 m distance from the building on opposite sides. The electrode resistances were 8.9 Ω (east) and 11.6 Ω (west) at the time of installation. The V-shaped path of the HV leads on the roof is indicated in Figs. 1(a) and 2. A 27-μH coil in series

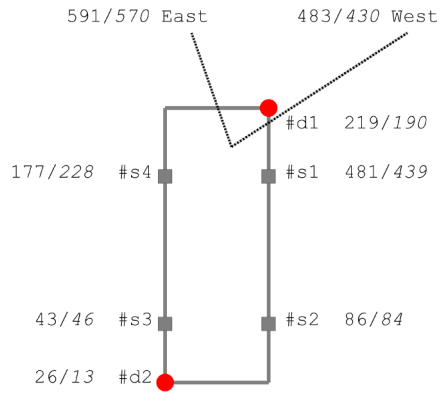

Fig. 2. Current distribution on the frame carrying the source. (Dashes) HV leads. (Dots #d1–2) Connection of frame to roof grid. (Squares #s1–4) Conducting short pillars between frame and steel skeleton. The current values measured/*calculated* have been normalized to 1 kA at the source.

with the capacitor limited the current in case of an inadvertent short circuit.

To ensure linearity, the currents were measured with air-core Rogowski coils combined with active/passive integrators [12]. Pearson current probes, with a conversion factor of 0.1 V/A, are used for smaller currents. For the voltage measurements, we used standard probes and battery-powered digital scopes. The bandwidth of the current measurements is minimally several hundred kilohertz, sufficiently large to accurately record the transients.

Originally, we planned to increase the injection current gradually from 100 A up to 1.5 kA, only to be limited by accidental mishaps in other electronic systems. One cable loop of the fire detection system was mounted against the top floor ceiling, just under the roof LP grid and skeleton. The owners of the system imposed a maximum voltage induced in their system to 35 V or a CM current of 1 A, which was met by limiting the injection current to 0.3 kA. The test cables shared the supports with power and signalling cables of other systems that were operating (see

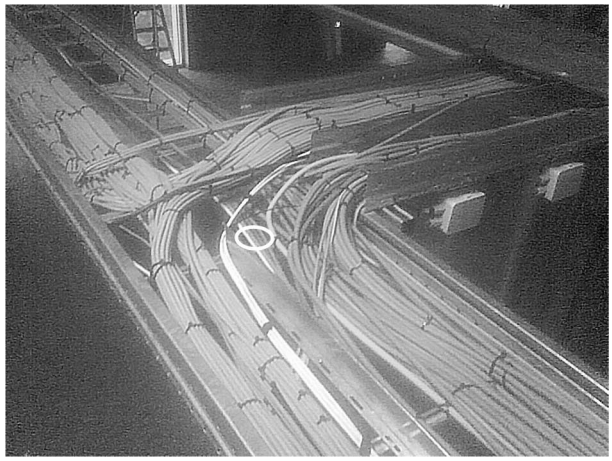

Fig. 3. Photograph of connection of three cable ladders. The white ellipse emphasizes the four test cables.

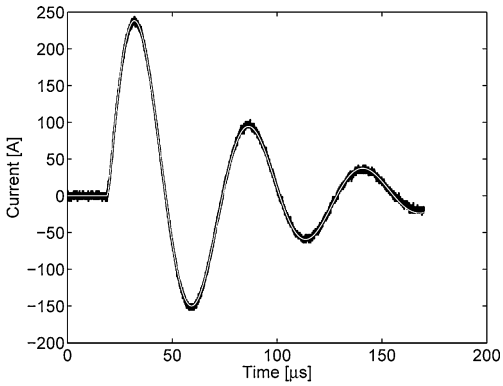

Fig. 4. Example of the current injected in the LP at the pharmaceutical plant. The white line shows the fit to a single *RCL* circuit.

Fig. 3). The switched-mode power supplies to which some of the other cables were connected generated quite some disturbances in the test cables. We improved the signal to noise ratio by averaging up to 100 records. This solution limited the number of measurements that could be performed in the available time. Experimental data in following sections will be scaled to the injection current of 1 kA.

III. Measurement Results

Fig. 4 shows an example of the injected current and the fit assuming an *RCL* circuit. Circuit parameters can be derived from the known capacitor value $C = 0.5\,\mu$F and the fit parameters: the resonance angular frequency is $\omega_d = 1.15 \times 10^5$ s^{-1} or frequency $f_d = 18.4$ kHz, the self-inductance $L = 150\,\mu$H, and the resistance $R = 5.11\,\Omega$. The resistance can be fully attributed to the grounding electrodes, which leaves no resistance for the building. This confirms the statement (see Section I) that induction determines the current distribution in the building. The peak current varied less than 10% over many discharge cycles.

Fig. 1(a) includes the peak currents through the connections between the LP grid and the steel frame at the building edge, normalized to a source current of 1 kA. The total measured current at the roof edge connections is 6% of the source current.

TABLE I
Cables Parameters: The Three-Lead Unshielded Power Cable, the Armored Twin-Lead Power Cable, and the Fieldbus Cable

Type	R'_{dc} [Ω/km]	$\lvert Z'_t \rvert$ (18 kHz) [mΩ/m]	I_p [A]	V_p [V]	Conf.
a) 3-ld.	6.8	31.	0.19	0.68	T
b) arm. 2-ld	7.41	17.4	0.025	0.054	V
c) fieldbus	9.5	12.	0.031	0.025	V
c) ,,			0.32	0.28	T

Current and voltage data in the first and last row have been measured with the T-shaped HV leads on the roof, the other two with the V-shape as in Fig. 2.

As a general trend, the current returns near the source and under the HV leads (see also [2]). The phase reversals found at several connections are remarkable and may indicate that isolated loops are present under the roof.

Fig. 2 presents the currents leaving the frame under the source toward the skeleton (#sn) and toward the roof grid (#dn), and the currents through both HV leads. One observes that about 80% of the current flows toward the skeleton that acts as a bypass for the grid. The remaining 14% leaves the grid at other connections with the skeleton such as at the other frames, the thick lines in Fig. 1(a).

The current through the cable support was measured at only one position, with a T-shaped layout of the HV leads directly on the roof instead of the V-shape, as in Fig. 1(a). The value of 11 A/kA injection is also indicated in Fig. 1(c).

At the far end of the 100 m test cables, all PE leads and shields were short-circuited to the cable support. Here "far" means as viewed from the measuring equipment. At the near end, the cable shield and/or PE lead were again connected to the support. The loop formed by the PE and the support can be considered as the CM current loop. At the near end, we measured the CM current and also the voltage induced between all other leads bundled together and the PE. If one considers the bundled leads as a single one, the voltage can be viewed as a differential mode (DM) with respect to the PE or shield. The DM voltage and CM current relate via a transfer impedance Z_t. Peak values of the 18.4 kHz component in CM current and DM voltage are summarized in Table I, normalized to 1 kA source current.

We also measured the transfer impedances Z'_t in the laboratory on 1 m long cable samples, as detailed in [13]. A vector network analyzer has been used for frequencies of 300 kHz and higher, and a combination of a signal generator and lock-in detector for frequencies below 1 MHz. Fig. 5 shows the results for three cables selected as examples as follows:

a) a 3×2.5 mm^2 power cable with one PE lead;
b) a twin lead 2×2.5 mm^2 cable with steel armor and a 2.5 mm^2 copper litz as PE lead embedded in it; the armor has eight bundles of two wires of 0.3 mm diameter wound clockwise and eight bundles of eight wires in the opposite direction;
c) a "Profibus" fieldbus [14] cable for data transport with two 0.7 mm diameter copper leads inside a shield composed of an aluminum foil and spacious copper braid consisting of 16 bundles of five 0.15 mm diameter copper wires.

For cable a, one has

$$Z'_t = R'_{\rm dc} + j\omega M' \tag{1}$$

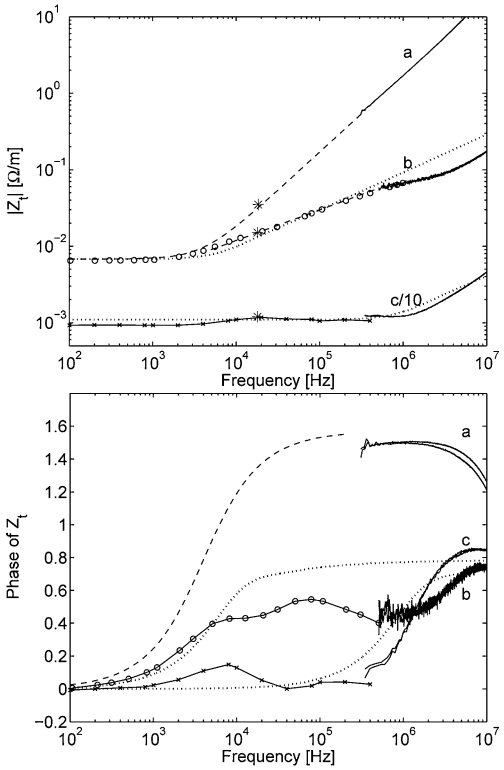

Fig. 5. Measured transfer impedance of the three lead power cable a, the armored two lead power cable b, and the fieldbus c, in amplitude (top) and phase (bottom). The dotted lines are the approximations used for the extrapolation (see Section V). The markers $*$ show the $|Z_t'|$ values for the 100 m test cables.

Fig. 6. Samples of (top) the armored twin lead power cable and (bottom) the shielded Profibus cable.

with $R'_{\rm dc} = 6.8$ mΩ/m is the resistance of the PE lead, ω is the angular frequency, and $M' = 0.27\mu$H/m is the mutual inductance. The dashed line interpolates between the measured dc value and the high frequency Z_t'. The crossover frequency $R'_{\rm dc}/2\pi M'$ is 4 kHz.

The construction of cables b and c is displayed in Fig. 6. Because of the armor or braid and foil outermost conductor, their $|Z_t'|$ rises much slower than cable a above 10 kHz. The $|Z_t'|$ of cable b rises proportional to $\omega^{0.4}$ (dashed line) between 5 and 500 kHz; the phase angle is about $\pi/6$. Above 1 MHz, $|Z_t'|$ tends to rise $\propto \omega^{0.5}$ and the phase approaches $\pi/4$, appropriate for a Z_t' dominated by the skin effect. The fieldbus $|Z_t'|$ is nearly flat up to 2 MHz and increases proportionally to $\sqrt{\omega}$ at higher frequencies, whereas the phase tends to $\pi/4$. This behavior is analogous to the skin effect surface impedance, but it is rather unexpected for a cable with a foil shield. The small change in amplitude and phase near 10 kHz is tentatively attributed to the magnetic field penetration of the aluminum shield caused by the slit; a detailed investigation is outside the scope here. The ratio of measured peak current (I_p) and voltage (V_p) on the 100 m test cables in the building agrees with the respective cable Z_t's at the injection frequency, as indicated by the markers in Fig. 5.

IV. Modeling

In order to reduce the complexity of the model, a limited number of conductors was taken into account, selected for their intended or probable contribution to LP.

A. Overall Structure

The model starts with the conductors shown in Fig. 1 implemented in a commercial method of moments (MoM) code [15] (see also [16]). The 50 mm^2 copper LP grid on the roof at 19 m height consists of meshes of approximately 20 m by 10 m. In Fig. 1(a), the grid and frames of the air-conditioning units are shown. Fig. 1(b) shows the horizontal part of the steel skeleton at 0.5 m below the roof grid. The skeleton consists of I-beams (thick lines) modeled as 20 cm diameter tubes and diagonal flat girders (thin lines) modeled as 10 cm diameter tubes. Vertical tubes of 20 cm diameter were included along the skeleton edge and extended downward. The layout of the cable support is shown in Fig. 1(c). As the model for the cable ladder, we choose two tubes of 7.4 cm diameter and one middle beam of 6.4 cm diameter, 2.5 m below the roof grid; the cables were not included in the overall model. The vertical part of the paths is not shown in the figures. Fig. 2 shows the frame carrying the source in more detail. The dotted lines indicate the HV leads (diameter of 1.5 mm) in the V-shape configuration. A single 18 kHz voltage source is assumed between the HV leads junction and the frame. At the ends of the HV leads, the actual resistors (see Section II) have been assumed. At four points (squares), the frame rests on the steel skeleton via short-conducting pillars. In view of the actual low resistance to ground (see Section II), the soil under the building is regarded as a perfect conductor. A large amount of other metal present is neglected in this first model. All MoM segments have a maximum length of 4.5 m, and the total number of segments is about 5000. We tentatively introduced skin effect assuming a resistivity $\rho = 10\,\mu\Omega$·cm of steel, relative permeability $\mu_r = 200$, and skin depth $\delta \approx 0.1$ mm. The currents varied less than 1% compared to the perfect conductor case. We did not consider skin effect further.

The calculated impedance seen by the 18 kHz, 1 kA source is $5.04 + j11.25$ V/A. The imaginary part is equivalent to an inductance of 97 μH. If the 27 μH of the series coil is added, the total inductance is in reasonable agreement with the 150 μH from the fit on the measured current (see Section III). The distribution of current over both HV leads agrees well with the measurements, as indicated in Fig. 2. It should be noted that the HV lead currents have been measured separately from the source current, and minor variations occurred between discharges. The same good agreement holds for the distribution of current over the frame connections with the grid and the steel skeleton: the skeleton carries 80% of the current. Several

connections between grid and steel skeleton were distributed over the roof, but these were not included in the model. As a result, the calculated sum of the currents toward the skeleton at the roof edge is 183 A, much larger than the 60 A measured. No phase reversals were found in the model.

The cable support current at #1 in Fig. 1(c) is 30 A in the model with the T-shape for the HV leads. This is nearly a factor of three larger than measured. A 0.8-m-diameter air duct ran close above the cable support. The duct was not an intended conductor because of rubber gaskets between the elements. However, the many bolts and metallic suspensions to the building structure made it a probable continuous conductor. When included in the model over the length of sections #1 and #3 in Fig. 1(c), the duct reduced the support current to 17 A. With this result, we decided not to include more conductors in the model.

The reinforced concrete roof plate were omitted in the model. The grids of different plates were physically separated and insulated. Such grids have a local effect, but do not contribute to the overall protection.

We verified that the current distribution remained the same when the frequency was increased from 18 to 180 kHz. This was to be expected, because induction determined the current distribution rather than the resistance at the grounding electrodes. We verified that the current 20%–80% distribution between roof grid and skeleton did not depend on the HV leads. A Web-like structure of 12 HV leads evenly distributed over the building showed the same ratio. Actually, we would have preferred such an injection circuit for the measurements. The effect of a solid conducting floor has been studied in [17]. We also included a metallic layer on the fourth floor; it left the current distribution above it nearly unchanged. However, equipment at floors below will see some benefit from it.

B. Cable Support Details

The cable ladders have rungs with 0.2 m separation. Many other cables share the support with the test cable bundle, but first we consider the latter only. The actual cross section of the ladder beams is shown in Fig. 7. The diameters in the overall model have been chosen to give an identical current distribution. The four test cables are taken as a bundle of 2 cm diameter, short circuited to the support at both ends. A 2-D static MoM code [18] resulted in the current distribution by requiring zero magnetic flux between the conductors. Rungs in the ladders short circuit the beams and reduce the magnetic flux through the openings. Because of the zero flux requirement in the MoM, one may omit the rungs. The part of the current through the test cable bundle is shown in Fig. 7 as a function of the bundle position over the dashed line. Many other cables share the support. We included four bundles of such cables in the same model, while the test bundle was placed close to the middle beam, the position shown in Figs. 3 and 7. The current part through the test cable bundle decreased by a factor of three. The measured ratio was 10% at branch #1 in Fig. 1(c). The model underestimated the cable bundle current. Again here, there remain many unknowns: variations in support (trays and ladders), in position and presence of other cables, and their unknown terminations and possible pigtails.

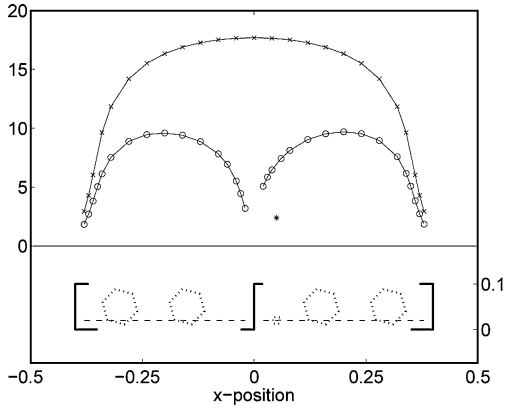

Fig. 7. (Top) Test cable bundle current as a function of the position of the bundle, as percentage of the total current through the cable bundle and support, with (o) and without (x) the middle beam present. The marker ∗ shows the value and position with four other bundles added (see Section IV-B). (Bottom) Ladder beams (heavy lines) and assumed positions of cable bundle (dashes) for the top part. The dotted lines indicate the four other bundles.

TABLE II
CALCULATED CURRENT IN AMPERE THROUGH THE CABLE SUPPORT FOR A LIGHTNING CURRENT OF 1 KA ATTACHED AT POINTS L1, L2, AND L3 [SEE FIG. 1(A)]

Position	#1	#2	#3
L1: Corner	10.1 / 7.8	6.1 / 5.2	3.9 / 2.5
L2: Inj. source	1.3 / 2.1	4.0 / 3.7	2.8 / 2.0
L3: Cable support	31.2 / 26	17.3 / 16	13.8 / 9.6

The data are presented without/with air duct.

C. Lightning Simulation

A 200-m-tall vertical current path is assumed as the model for the lightning channel. An 18 kHz voltage source with high internal impedance is positioned at half-height. The lower path connects the source and the building, the upper path is a free-standing antenna on top of the source. The current in upper path closes via the displacement current; most of the displacement current flows toward the soil. Three positions were chosen as attachment points to the building [see Fig. 1(a)]; L1 is at the corner of the building, L2 at the measurements injection point, and L3 on the roof edge exactly above the end of the branch #1 of the cable support. For the L1 position, the displacement current part on the building was determined as the difference between the current arriving at the corner and the sum of the conduction currents leaving via the connections to ground. The displacement current amounted to 3% of the injected current. In case of attachment at L2, the skeleton/grid current ratio remained 80% to 20%, and similar values in case of L1 and L3. The currents in the three support branches (#1, #2, and #3) are given in Table II. The horizontal air duct has only a small effect compared to the case of current injection with the HV leads.

V. TENTATIVE SCALING TO LIGHTNING

Under the assumption that the current distribution does not change, the model can be scaled up to the lightning parameters

TABLE III
MODEL PARAMETERS OF FIRST AND SUBSEQUENT LIGHTNING STROKE, AFTER [1]

	first			subsequent		
Parameter	I	II	III-IV	I	II	III-IV
I [kA]	200	150	100	50	37.5	25
k		0.93			0.993	
τ_1 [μs]		19			0.454	
τ_2 [μs]		485			143	

given in [1, Part 1, Annex. B]. The transfer impedances of the test cables translate the currents into voltages that would be shared by equipment at both ends of the cables. Conservative values are obtained by taking the highest cable support current (#1 and L3 without air duct in Table II) and the measured 10% for the cable bundle (see Section IV-B). The finite-wave velocity over the supports and cables, and possible resonances have not been taken into account. Such effects could, in principle, be handled as detailed in [19] and [20]. Measurements showed that the bundle current is divided in a 3:3:2:2 ratio between two power cables and two thinner signal cables. A 200 kA lightning current pulse with 10 μs rise time, corresponds to severity level I (see Table III) for the first return stroke. The approximating expression for the lightning current i reads [1]

$$i(t) = \frac{I}{k} \times \frac{(t/\tau_1)^{10}}{1 + (t/\tau_1)^{10}} \exp(-t/\tau_2). \tag{2}$$

The corresponding front and tail time constants are τ_1 and τ_2, respectively. The 200 kA lightning induces 6 kA in the support and 180 A in a power cable. The temperature rise of any of the cables is less than a degree Celsius. The Z_t' of three cables of Table I has been modeled by (1) for cable a and by a skin effect surface impedance approximating the data for cable b and c in Fig. 5

$$Z_t' = R_{\rm dc}' \frac{xJ_0(x)}{2J_1(x)} \tag{3}$$

with $R_{\rm dc}'$ is the dc resistance per meter length, J_n is the Bessel function of order n, $x = \sqrt{-jf/f_\delta}$, and f_δ is the characteristic frequency, where the skin effect sets in (see also [13]). The measured Z_t' of cables b and c is more complex than (3); at high frequencies the fit overestimates the measured $|Z_t'|$ (see Fig 5). The current has been converted into the frequency domain by a Fourier transform over 2×10^5 points with 0.1 μs time step, and then multiplied by the transfer impedances. The resulting voltage has been converted back into time domain by an inverse transform. The initial parts of the voltage waveforms are shown in Fig. 8. Calculated induced peak voltages are given in Table IV, together with the voltages corresponding to the subsequent return stroke calculated similarly (50 kA, 0.25 μs rise time, 10^6 points with 10 ns time step).

Please note that the voltages are those between the power or signal leads taken as a bundle, with respect to the PE lead or shield. The peak voltage induced in the unshielded cable a by a subsequent stroke could pose a problem for the equipment. The value is fully determined by the time derivative of the current in (2). All other values are within safe ranges. For instance, with the armored cable *b* the voltage is a factor of 3 or 20 lower than

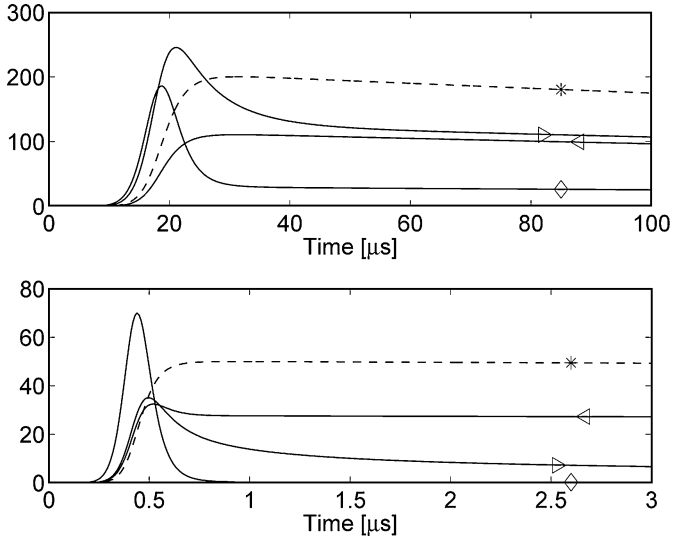

Fig. 8. Initial part of the waveforms for current and voltage. (Top) First stroke lightning current (* dashed, in units of kA) and voltages on three-lead cable (◇, divided by four), armored cable (▷), and fieldbus cable (◁). (Bottom) Subsequent stroke lightning current (* dashed, in units of kA) and voltages on three-lead cable (◇, divided by 100), armored cable (▷, divided by ten), and fieldbus cable (◁). At times larger than shown by the graphs, the voltages approximately follow the current.

TABLE IV
PEAK CABLE CURRENTS AND VOLTAGES CALCULATED FOR THE FIRST AND SUBSEQUENT LIGHTNING STROKE, ATTACHED AT POINT L3 [SEE FIG 1(A)]

	first		subsequent	
cable	I_p [kA]	V_p [kV]	I_p [kA]	V_p [kV]
a) 3-ld.	0.18	0.74	0.045	7.0
b) arm. 2-ld	0.18	0.25	0.045	0.35
c) fieldbus	0.12	0.11	0.030	0.032

The cable length is 100 m; propagation time and resonance phenomena are not considered.

cable a, for the first and subsequent stroke, respectively. The voltage between the power or signal leads is often one or two orders of magnitude lower than those calculated here [21].

The values of Table IV result from a direct extrapolation, neglecting travel times and resonances. The cable support is attached to the building structure through many wires, randomly spread with distances of the order of 3 m. This mesh of conducting interconnects is not included in the calculations. The local circuits resonate at frequencies of 50 MHz and up. The travel time of a current wave over the cable support and nearby building structure is about $0.3\,\mu$s, and subsequent strokes with rise time of 0.25 μs can excite resonances. Analogous to the overshoot of an *L–C–R* resonator, a factor of two increase in current may be expected. A similar current increase has been observed due to ground reflections on tall buildings [22]. The voltages of Table IV increases less because of the different travel time inside and outside the cable. A more detailed analysis is not warranted for this model of the building. Nevertheless, the resonance excitation [23] is the subject of current investigations.

VI. CONCLUSION

The LP system on the roof of a new plant has been tested by measurements, and a MoM model has been used to extrapolate

to lightning currents. The MoM model correctly produces the current distribution between the roof grid and the skeleton. This distribution is mostly determined by the local magnetic coupling. The lightning capture rods are connected to the grid. In case of a stroke on such a rod midroof, the grid will be important. But in all other cases, the denser and heavier building skeleton appears to be a better LP. The model presented overestimates the cable support current by a factor of three when compared to the measurements; a factor of 1.6 when including the air duct. Even assuming the larger support current, the cables appear well protected.

Cable bundles have been intensively studied elsewhere, e.g., [24]. When manufactured in large numbers such as in the automobile industry, a large effort in the modeling is justified. In a building, as discussed here, one has to accept the "as built" situation. To retrieve the actual composition of the cable bundles and the individual cable connections required a number of man-hours that was unavailable for this study. In addition, incomplete knowledge about the building details remained, such as other metal and the interconnections. The uncertainty of the model is more due to the available input than to the MoM itself. In a comparable low-frequency calculation, where analytical expressions for the fields were available, an accuracy of better than 2% could easily be achieved [25] using the same software. Still, the limited model applied gave acceptable results and good indications as to the lightning safety of the installations.

The measurements on the Z_t show the benefits of armored/shielded cables even inside buildings.

ACKNOWLEDGMENT

The authors would like to thank Organon–Oss (Schering–Plough at the time of writing) for the permission to carry out the measurements. We would also like to thank H. Broekmeulen and R. Parrado-Curros for their assistance in the preparation and during the measurements.

REFERENCES

[1] *Protection Against Lightning*, IEC 62305, 2006.
[2] W. Zischank, F. Heidler, J. Wiesinger, I. Metwally, A. Kern, and M. Seevers, "Laboratory simulation of direct lightning strokes to a modeled building: Measurements of magnetic fields and induced voltages," *J. Electrostatics*, vol. 60, pp. 223–232, 2006.
[3] A. Kern, F. Heidler, S. Seevers, and W. Zischank, "Magnetic fields and induced voltages in case of a direct strike — Comparison of results obtained from measurements at a scaled building to those of IEC 62305-4," *J. Electrostatics*, vol. 65, pp. 379–385, 2007.
[4] I. Metwally, F. Heidler, and W. Zischank, "Magnetic fields and loop voltages inside reduced and full scale structures produced by direct lightning strikes," *IEEE Trans. Electromagn. Compat.*, vol. 48, no. 2, pp. 414–426, May 2006.
[5] *Electromagnetic Compatibility, Part 5: Installations and Mitigation Guidelines; Section 2: Earthing and Cabling*, IEC61000-5-2, 1997.
[6] A. van Deursen, IEC 61000-5-2: Electromagnetic compatibility, Part 5: Installations and mitigation guidelines; Section 2: Earthing and cabling, Eindhoven Univ. Technol., Eindhoven, The Netherlands, EUT Rep. 93-E-275, 1993.
[7] A. van Deursen, J. Wetzer, and P. van der Laan, "Local protection of equipment in high voltage substations," presented at the 6th Int. Symp. High Voltage Eng., New Orleans, LA, 1989, Paper 31.03.
[8] P. van der Laan and A. van Deursen, "Reliable protection of electronics against lightning: Some practical applications," *IEEE Trans. Electromag. Compat.*, vol. 40, no. 4, pp. 513–520, Nov. 1998.
[9] G. Ala and M. Di Silvestre, "A simulation model for electromagnetic transients in lightning protection systems," *IEEE Trans. Electromagn. Compat.*, vol. 44, no. 4, pp. 539–554, Nov. 2002.
[10] G. Bargboer, A. van Deursen, C. Nguyen, H. Steenstra, T. Bosveld, R. Parrado Curros, and J. Broekmeulen, "Finding weak spots in lightning protection," in *Proc. Int. Symp. EMC (EMC Eur. 2008)*, Hamburg, Germany, Sep., pp. 269–274.
[11] G. Bargboer and A. van Deursen, "Lightning protection of a pharmaceutical plant, measurements and modeling," presented at the ICEAA 2009, Torino, Italy, Sep.
[12] A. van Deursen, H. Smulders, and R. de Graaff, "Differentiating/integrating measurement setup applied to railway environment," *IEEE Trans. Instrum. Meas.*, vol. 55, no. 1, pp. 316–326, Feb. 2006.
[13] H. Steenstra and A. van Deursen, "Reduction of conducted interference by steel armor in buried cables: Measurements and modeling," *IEEE Trans. Electromagn. Compat.*, vol. 50, no. 3, pp. 678–686, Aug. 2008.
[14] (2010). [Online]. Available: http://www.profibus.com
[15] *FEKO User's manual*, FEKO, Stellenbosch, South Africa, 2008.
[16] (2010). [Online]. Available: http://www.feko.info/
[17] S. Miyazaki and M. Ishii, "Role of steel frames of buildings for mitigation of lightning-induced magnetic fields," *IEEE Trans. Electromagn. Compat.*, vol. 50, no. 2, pp. 333–339, May 2008.
[18] A. van Deursen, F. van Horck, and J. van der Merwe, "A self-optimizing discretization scheme for 2d boundary element calculations," *J. Electromagn. Waves Appl.*, vol. 15, no. 4, pp. 461–476, 2001.
[19] C. Baum, T. Liù, and F. Tesch, in *On the Analysis of General Muliconductor Transmission-Line Networks*. Iteraction Notes, Note 350, Nov. 1978.
[20] A. R. Djordjevič and T. K. Sarkar, "Analysis of time response of lossy multiconductor transmission line networks," *IEEE Trans. Microw. Theory Tech.*, vol. MTT-35, no. 10, pp. 898–908, Oct. 1987.
[21] B. Demoulin, S. Assad, and P. Degauque, "Analysis of the behavious of a shielded two-wire line in a disturbing environment," presented at the 7th Int. Zurich Symp. EMC, Zurich, 1987, Paper 34F6.
[22] V. A. Rakov, "Transient response of a tall object to lightning," *IEEE Trans. Electromagn. Compat.*, vol. 43, no. 4, pp. 654–661, Nov. 2001.
[23] C. Baum, "From the electromagnetic pulse to high-power electromagnetics," *Proc. IEEE*, vol. 80, no. 6, pp. 789–817, Jun. 1992.
[24] G. Adrieu, A. Reinex, X. Bunlon, J. Permantier, L. Koné, and B. Démoulin, "Extension of the "Equivalent Cable Bundle Method" for modeling electromagnetic emissions of complex cable bundles," *IEEE Trans. Electromagn. Compat.*, vol. 51, no. 1, pp. 108–118, Feb. 2009.
[25] A. van Deursen and V. Stelmashuk, "Sensors for in-flight lightning detection on passenger aircrafts," presented at the ESA Workshop Aerosp. EMC, Florence, Italy, Mar. 30– Apr. 1 2009.

Geesje Bargboer (S'06) received the B.Sc. degree in electrical engineering with the specialization in telecommunication from Saxion University of Applied Sciences, Enschede, The Netherlands, in 2001, and the M.Sc. degree from Eindhoven University of Technology, Eindhoven, The Netherlands, in 2006, where she is currently working toward the Ph.D. degree.

Her current research interests include electromagnetic compatibility of cabling and wiring in buildings and installations.

Alexander P. J. van Deursen (A'97–SM'97) received the Ph.D. degree in physics from Radboud University, Nijmegen, The Netherlands, in 1976.

He was a Postdoctoral Researcher at the Max Planck Institut fur Festkörperforschung, Hochfeld Magnetlabor, Grenoble, France. He was engaged in solid-state physics on electronic structures of metals, alloys, and semiconductors by high magnetic field techniques in Nijmegen. In 1986, he joined the Eindhoven University of Technology, Eindhoven, The Netherlands, where he is involved in electromagnetic compatibility (EMC).

Dr. van Deursen has also been engaged in several International Electrotechnical Commissions working groups. He has been the Chairman and a member of different committees in international conferences. He is a member of the International Steering Committee of EMC Europe.